

# Attenuation Correction and Three-Dimensional Filter of SPET Projections.

*H. Berrah, M. Bourguignon, B. Bendriem and A. Syrota.*

**Abstract-** To improve quantification of Single Photon Emission Tomography (SPET) data, an analytical attenuation correction using measured attenuation coefficient maps and applied on projections has been developed. Projections corrected from attenuation require the use of an efficient filter because they are affected by noise. A three-dimensional (3D) Fourier filter has been developed. It is based on the properties of the Fourier transform and on the relationship between spatial and angular frequencies. A significant improvement of the quantitative results (signal to noise ratio, resolution and contrast) has been observed on phantoms when compared to the routinely used filters. This method was also tested on cardiac and cerebral tomographic data.

## I. INTRODUCTION

A Single Photon Emission Tomography (SPET) image is the cross sectional representation of an object, reconstructed from a set of unidimensional projections. These projections are given by the attenuated Radon transformation [1].

As an ideal case the two opposite projections of a point source can be represented by Dirac delta function. However, in reality the two opposite projections are different from one another and less than the ideal projection. Every reconstruction algorithm which allows us to obtain images of the object is adapted to the ideal case. Real projections are different from idealized projections because they include effects from: attenuation, diffusion, collimation, angular resolution, spatial resolution, compromise between resolution and sensitivity, and noise.

To adapt real projections to different reconstruction algorithms, especially the filtered back-projection (FBP) algorithm, we will correct them before reconstruction to be as quantitatively close as possible to ideal projections. To improve quantification of SPET data we have developed an analytic attenuation correction applied to projections. Because the correction was sensitive to noise, a three dimensional filter was developed in the Fourier frequency domain.

## II. ATTENUATION CORRECTION

Emission tomography has two unknown parameters: attenuation and the distribution source of radioactivity in the object. The hardness problem (inverse of the Radon transform which takes into account the two unknown parameters of the object in SPET) has obliged researchers to ignore one of them

when they establish a SPET reconstruction algorithm.

This simplification has caused the appearance in the literature of many attenuation correction techniques which can be grouped into two basic methods: iterative and analytical. Iterative methods give good results, however the time of execution and convergency problems has limited their practical use. In analytical methods three principles are employed:

(1) homogeneous attenuation maps and homogeneous radioactivity distribution sources; results are quantitatively poor.

(2) homogeneous attenuation maps and heterogeneous radioactivity distribution sources ;quantitative results are better but remain unsatisfactory.

(3) Finally heterogeneous attenuation maps and homogeneous radioactivity distribution sources has been introduced [2].

### A. Attenuation maps

Transmission technique using an external source can provide real attenuation maps. Three set-ups for transmission have been described using either a point source (cone beam geometry) [3,4], a line source (parallel or fan beam geometry) [5] or a flood source (parallel geometry) [6]. They provide raw maps of  $\mu$  values for each voxel of the emission field. The transmission technique established in our laboratory [3] has a point source attached to an uncollimated gamma camera at a variable distance above a useful field of view. The field of view is defined by an obstructor, which eliminates the direct irradiation (i.e. without transmission) of the crystal.

The new attenuation correction is based on principle (3) above: it uses the linear attenuation coefficient maps of the object and the emission projections. A significant attenuation compensation projection is obtained by dividing each pixel value of the emission projections by the average of the attenuation factors ( $\exp(-\sum \mu)$ ) of all pixels along the same projection ray.

The method has been evaluated on various simulated projections (without attenuation, with attenuation, and with attenuation correction without and with noise) reconstructed using the filtered back-projection algorithm with the ramp filter.

### B. Modeling

To validate the new attenuation correction we have simulated cerebral and heart SPET data using RECLBL library.

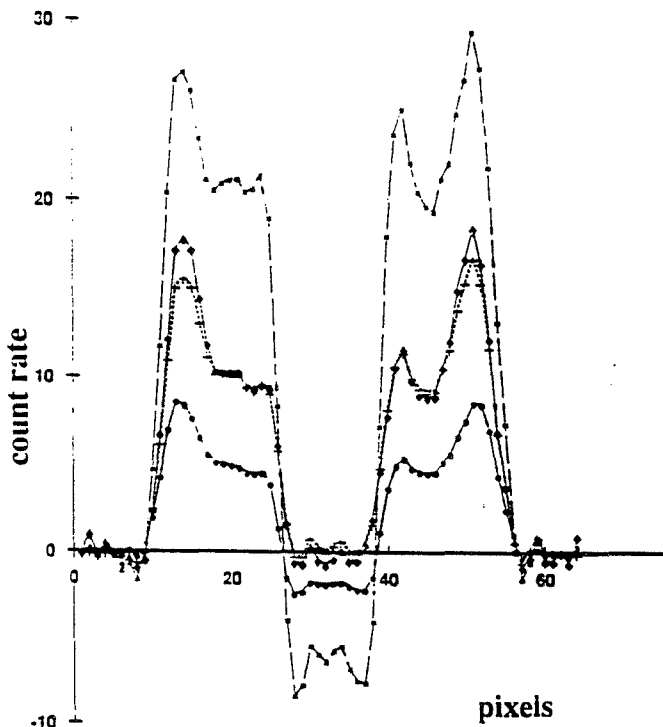
In the cardiac model, the myocardium, chest wall, lungs, mediastinum and spine received different activities and  $\mu$  values. In the cerebral model, the striata, cortex, white matter and skull also had different activities and  $\mu$  values. Detailed description of the modeling, algorithms and preliminary results are published elsewhere [2].

---

All authors are with Service Hospitalier F. Joliot, C.E.A.,  
4 Place du Général Leclerc, 91401 ORSAY FRANCE.  
Correspondance should be asked to first author.

### C. Results

Results obtained for noise-free projections are very satisfactory. The count rate in corrected noise-free projection is about 95% of the ideal projection (no attenuation) while before correction it was about 50% of the ideal projection. The standard deviation of the count rates of each transverse projection line contributing to one sinogram was used as a measure of the variability of the attenuation effect; ideally, it is equal to zero. After attenuation correction, the standard deviation decreases by a factor 2, indicating a significant improvement. After reconstruction by filtered back projection, the transaxial slices were also compared to the original model by means of count profiles obtained at different levels through the slice (figure 1); these profiles clearly demonstrate the quality of the correction method. However if we take a uniform map of linear attenuation coefficients (eq 0.15 cm<sup>-1</sup>) and we apply it in the corrected projection formula, we overestimate a hot region and underestimate a cold region (figure 1).



- Attenuated data
- Attenuated corrected data with constant  $\mu$  (\*) and  $\mu$  map (+)
- Unattenuated and noise free reference.

fig. 1 Profiles through reconstructed images of heart model.

### D. Introduction of noise

One of greatest problems in absolute quantification in SPET is a propagation of noise in each step of acquisition and reconstruction. A second phase of our work is to see if the new attenuation correction remain reliable in the presence of noise. The first component of noise is from emission and since our goal is to use maps of linear attenuation coefficients obtained from a transmission scan, a second component of noise will appear in the corrected projections from transmission data.

The number of counts  $N'$  in the simulated projections do

not take into account the count rate of emission and duration of acquisition. So a corrective factor was introduced to simulate a relative uncertainty similar to that found under experimental conditions.

This factors is called  $k_e$  for emission data and  $k_t$  for transmission data.

Gaussian noise was added to the attenuated projections and transmission maps. Gaussian emission noise was calculated using the standard deviation given by the multiplication of the square root of the attenuated projections by  $k_e$  and transmission noise by the multiplication of the square root of transmission maps projections by  $k_t$ . To increase statistics, this operation was repeated 30 times for all the values of  $k_t$  and  $k_e$ . The corrected attenuation projections resulting from these noisy data were reconstructed with filtered backprojection and Hamming-Hann windows. From one profile drawn on each of the 30 cases, the means and standard deviations were calculated.

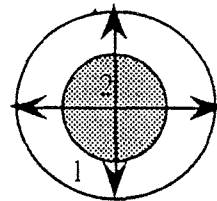
$$\text{Var}[p^c(\theta, x')] = \sum_{i=1}^n \left[ \frac{\partial [p^c(\theta, x')]}{\partial [p_i^a(\theta, x')]} \right]^2 \text{Var}[p_i^a(\theta, x')]$$

$$\text{if } p^c(\theta, x') = \frac{p^a(\theta, x')}{C(\theta, x')} \text{ then}$$

$$\text{Var}[p^c(\theta, x')] = \frac{1}{C(\theta, x')^2} \text{Var}[p^a(\theta, x')] + \left( \frac{p^a(\theta, x')}{C(\theta, x')^2} \right)^2 \text{Var}[C(\theta, x')]$$

$C(x', \theta)$  was the average of the attenuation factors,  $P^c(\theta, x')$  the corrected projection and  $\text{Var}$  the variance of the corresponded entities.

The relative importance of each component of noise was studied with a simulated cylinder. Simulations were obtained in the same way as previously described for cardiac and cerebral models.



- 1) Aqueous solution with an attenuated coefficient of 0.15 cm<sup>-1</sup> in the external ring (radius 22 cm).
- 2) Radioactive aqueous solution (activity 100 cps/pixels) contained in an elliptical cylinder (small axis 11 cm and large axis 12 cm)

fig. 2 Cylindrical phantom

### E. Results

Noise due to emission predominates at low count rates in the emission projections while the noise due to transmission has an effect only at high count rates (figure 3). When the mean value of noise is high in transmission data, the results are not acceptable in comparison with noise-free data, requiring

the use of a filtering of projections before attenuation correction.

Signal to noise ratio.

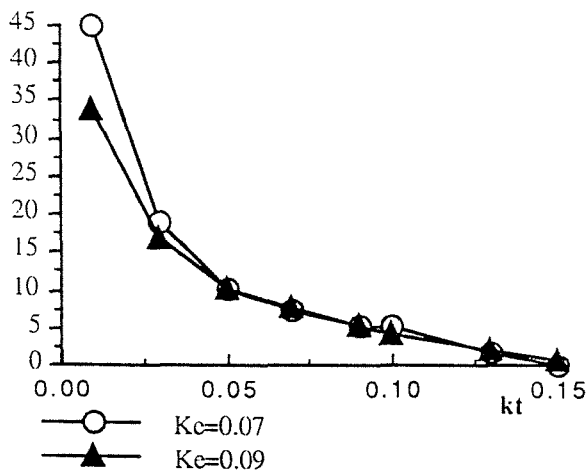
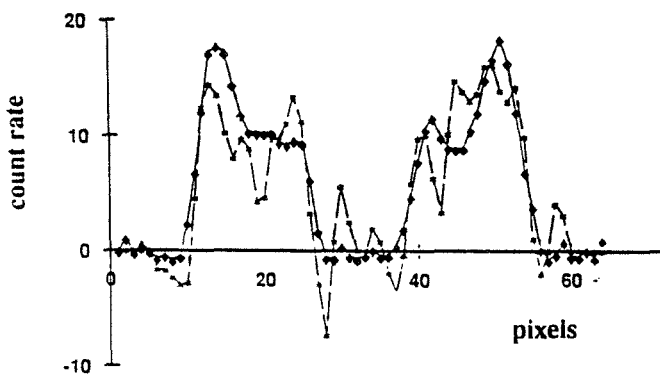


fig. 3 Signal to noise ratio plotted against emission and transmission statistics.

After reconstruction by FBP, the transaxial slices were compared to the original model and the ideal one by means of count profiles obtained at different levels through the slice. In figure 4 is an example of a profile showing good results after correction, although it is not as good as the results obtained in the absence of noise.



- Attenuated corrected images reconstructed from attenuated, noisy projections and noisy transmission.
- Unattenuated and noise free reference.

fig. 4 Profiles through reconstructed images of heart model.

#### F. Conclusion

The improvement in quantification using the new attenuation correction method is limited by the level of noise in both emission and transmission projections.

The method we propose does not exclude any complementary filtering since only the projections are corrected before reconstruction.

### III. 3D FOURIER FILTER

The optimal filter should not only improve the quality of

images by noise reduction but also preserve their quantification, i.e. obtain the maximum of exact information from a set of projections of the acquired object.

A spatial bidimensional fast Fourier transform (BDFFT) of an image creates an oversampling of frequency components by decomposing the transform signal into central value ( $v=0$ ), imaginary and real parts with a step size twice smaller than that of the entire signal transform. Furthermore, the relationship between spatial and angular frequencies in SPECT (Lindgren and Rattey -1981) combined with the properties of BDFFT allows to obtain an oversampling in 3D.

Since Poisson noise related to radioactive counting is not periodic and cannot be periodized, a Fourier series truncated to a limited number of harmonics represents a clever filtering of a radioactive periodic signal. Consequently, a three dimensional filter established in the Fourier frequency space can tackle the high frequency components of noise and quantitatively preserves the 3D nature of SPECT data by using the relationship between spatial and angular frequencies. Periodicity can be obtained in SPECT in the transverse direction by masking the object by a rectangular region of interest in each projection.

#### A. Algorithm

The 3D Fourier filter algorithm is the following: Bidimensional spatial frequencies are obtained by taking the Bidimensional Discrete Fast Fourier Transform (BDFFT) of images while filtering in the third direction will be obtained by a Fourier series of the amplitudes of each BDFFT frequency.

(1) Linograms (so called due to their shape) are first obtained from a geometrical transformation of a set of masked projections, the dimensions of which are  $z$ , the patient axis, and  $\theta$ , the angle of rotation. The 3rd dimension, the transverse direction  $r$  of the patient, is a periodic axis.

(2) Real and Imaginary frequency frames of each 2D linogram are obtained by BDFFT and considered as independent series.

(3) Amplitudes of each frequency signal are developed into a Fourier series in the  $r$  direction; truncation to an appropriate number of harmonics (e.g. 12 harmonics) allows a significant reduction of noise.

(4) An inverse BDFFT is applied to filtered Real and Imaginary frequency frames to obtain filtered linograms.

(5) Geometric inverse transformation is finally done to recover filtered projections.

#### B. Validation of the 3D nature of the filter

To assess the Three-dimensional nature of the Fourier filter, frequency frames obtained from a SPET study by 3 different processings were compared:

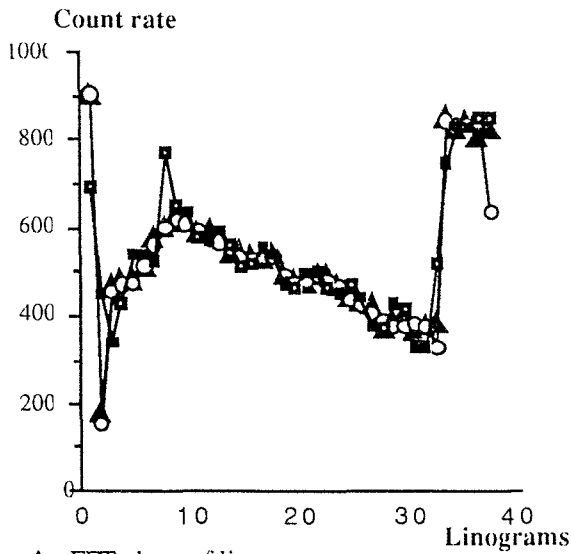
(1) Phases and amplitudes of linograms,  
 (2) These phases and amplitudes further filtered independently by a Fourier series.

(3) A Fourier series applied first to the linograms and the phases and amplitudes taken from the result.

The number of harmonics taken into account was 10.

Profiles of phases for these three cases are presented in figure 5. They appear quite different, demonstrating the application of a Fourier transformation to the linograms into  $\theta$  and  $z$ , followed by a Fourier series into  $r$ , is not a linear

operation. This is due to the correlation between  $r$  and  $\theta$ .



▲ FFT phase of linogram.  
○ After filtering by a Fourier serie.  
■ Fourier series applied to FFT phase of linogram.  
fig. 5 Profiles of phases.

### C. Experimental validation

A quantitative comparison between the Fourier filter and standard filters (Hamming-Hann, Butterworth and Wiener) has been performed.

#### - Application to a resolution phantom.

Two acquisitions of 1 sec and 8 sec per projection of a multiple line source phantom have been made. Each line source had the same diameter, less than 1mm or 0.22 pixels, and were filled with an aqueous solution of Tc 99m [figure 6a].

Vertical or horizontal resolution was taken by the FWHM about a vertical or horizontal profile of each line source on each filtered image. We used a zoom of 2 to have a high spatial sampling at the expense of lower count rates per pixel.

To rule out the statistical variations of the point spread function in the tomographic acquisition, we compared the previous data with an additional acquisition of 30 sec per projection, reconstructed with a ramp filter alone as a reference and compared to reconstruction with apodisation window of Hamming-Hann and the 3D Fourier filter using 20 harmonics.

Results are given in tables 1 and 2.

### RESOLUTION VALUES FOR DIFFERENT COUNT RATE

#### Line Source Phantom

Vertical Resolution in pixels (= 4.54 mm)

Sources/ Filters	1	2	3
NH=6 1s	5.04	5.85	4.43
NH=8 1s	4.66	4.71	3.07
NH=10 1s	4.99	4.12	4.37
Hamming-Hann 1s	5.05	4.34	5.00
Hamming-Hann 8s	4.75	4.20	3.86

table (1)

### RESOLUTION VALUES FOR HIGH COUNT RATE

#### Line Source Phantom

Horizontal resolution in pixels

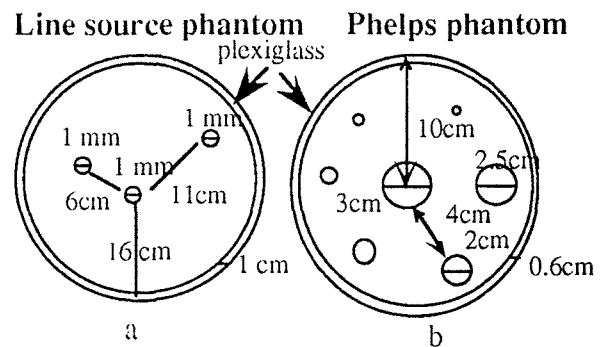
Sources/Filters	1	2	3
Ramp	5.46	5.30	5.64
NH = 20	5.60	5.75	5.84
Hamming-Hann	6.54	6.60	6.78

30 sec acquisition per projection.

table (2)

- The 3D Fourier filter resolution is similar to the ramp filter. Thus the Fourier filter truncates the high frequencies without creating aliasing.

- The Hamming-Hann filter for high count rate situations decreases resolution, however for a lower count rate the resolution was aberrant (it gave a resolution lower than the system resolution). This was possible because the Hamming-Hann filter and Butterworth filter have some oscillations on both sides of the central peak of their point spread functions, which contain negative amplitudes, resulting in an aberrant resolution in the reconstructed object.



Rotation radius of Gamma camera is 23 cm

fig. 6 Phantoms

#### - Application with a Phelps phantom

A second experiment was performed to study the effect of the Fourier filter on image contrast. We performed two acquisitions with a Sophy Camera DSX of a Phelps phantom (figure 6b) with cold rods (1 sec per projection and 20 sec per projection). For each image we chose 4 identical regions of interest (2x2 pixels), three of them were taken in three cold rods of Phelps phantom and the fourth one in the hot region.

The same images and the same ROI positions were used for each filter.

The contrast was measured as a ratio of the counts in cold region to the counts in hot region. In fact the ROI size was defined for the central rod and was subsequently applied to the other rods. Thus, the measured contrast was accurate only for the central rod.

Results are given in tables 3 et 4.

## CONTRAST VALUES FOR DIFFERENT FILTERS

### Phelps Phantom

Contrast for 1sec per projection

ROI / Filters	R1	R2	R3
Hamming-Hann	0.102	0.331	0.447
Butterworth 6/16	0.035	0.276	0.390
Wiener	0.034	0.276	0.390
NH=6	0.081	0.550	0.569
NH=8	0.007	0.402	0.575
NH=10	0.009	0.340	0.469

table (3)

Contrast for 20sec per projection

ROI / Filters	R1	R2	R3
Hamming-Hann	0.256	0.410	0.659
Butterworth 6/16	0.216	0.349	0.634
Wiener	0.217	0.415	0.605

NH: number of harmonics

The lower the value, the better the contrast

table(4)

The central rod contrast was better for the Fourier filter than for all other filters used. However, at low count rates, the contrast of the two other rods (R1, R2) for the Wiener filter images were slightly better than or equal to the contrast in the Fourier filter images. This can be explained by the Wiener filter principle, which amplifies middle frequencies beyond 100%, and causes increased contrast in that region by a refocusing effect.

- Finally, images obtained with the 3D Fourier filter on the Phelps phantom with an average count rate per projection of 50/pixel were visually identical with images obtained with a count rate of 1000/pixel, both reconstructed with an apodisation of Butterworth (figure 7).

The 3D Fourier filter was also applied to cerebral images of D2 receptors using I123 labelled ligands; it clearly demonstrated a better separation of the striata than any other filter.

## IV. CONCLUSION

The attenuation correction was successfully evaluated on low noise simulated projections, and the Fourier filter showed interesting noise reduction while improving resolution (linear source phantom) and contrast (Phelps phantom) for different levels of noise when compared to SPET filters. Their simultaneous application to both transmission and emission data is the next step to be performed.

## ACKNOWLEDGEMENT

The authors are very grateful to D. Raffel and H. Vallet for reading the manuscript.

## V. REFERENCES

- [1] De-Rosier DJ and Klug A. Nature, Lond, 217, 130, 1968.
- [2] Bourguignon M, Berrah H, Bendriem B and all.

Correction of attenuation in SPECT with an attenuation Coefficient Map: A new Method. J Nuc Biol Med, Vol 37, 1993

- [3] Bourguignon M, Vassiliou M. Disposition de scintillation utilisable pour l'atténuation par tomographie de transmission. Brevet français N° 89, 10225, 28 Juillet 1989.
- [4] Manglos H.M, Bassano D.A, Duxbury C E and Capone R B. Attenuation Maps For SPECT Determined Using Cone Beam Transmission Computed Tomography IEEE Trans Nucl Sci, Vol 37, N° 2, 600-608, 1990.
- [5] Bailey D L, Eberl S, Tan P, Meikle S R, Fulton R R and Hutton B F. Implementation of a scanning line source for attenuation correction with simultaneous emission/transmission SPECT. J Nuc Med, May, Vol 33, N° 5, 901, 1992.
- [6] Malko J A, Van Heertum R L, Gullberg G T and Kowalsky W P. SPECT Liver Imaging Using An Iterative Attenuation Correction Algorithm And An External Flood Source J Nuc Med 27, 701-705, 1986.

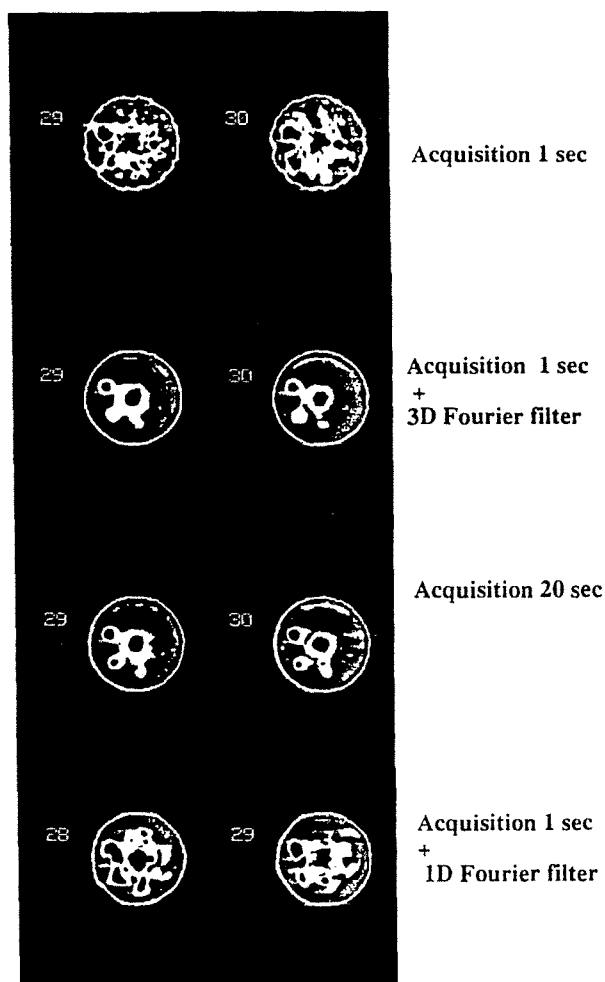


Fig. 7 Phelps phantom reconstructed by filtered backprojection apodisation by Butterworth 4/6